

Learning When to Use Adaptive Adversarial Image Perturbations against Autonomous Vehicles

Hyung-Jin Yoon¹, Hamidreza Jafarnejadsani², and Petros Voulgaris¹

Abstract—The deep neural network (DNN) models for object detection using camera images are widely adopted in autonomous vehicles. However, DNN models are shown to be susceptible to adversarial image perturbations. In the existing methods of generating the adversarial image perturbations, optimizations take each incoming image frame as the decision variable to generate an image perturbation. Therefore, given a new image, the typically computationally-expensive optimization needs to start over as there is no learning between the independent optimizations. Very few approaches have been developed for attacking online image streams while considering the underlying physical dynamics of autonomous vehicles, their mission, and the environment. We propose a multi-level stochastic optimization framework that monitors an attacker’s capability of generating the adversarial perturbations. Based on this capability level, a binary decision attack/not attack is introduced to enhance the effectiveness of the attacker. We evaluate our proposed multi-level image attack framework using simulations for vision-guided autonomous vehicles and actual tests with a small indoor drone in an office environment. The results show our method’s capability to generate the image attack in real-time while monitoring when the attacker is proficient given state estimates.

Index Terms—Adversarial Machine Learning, Reinforcement learning, Autonomous Vehicle

I. INTRODUCTION

Machine learning (ML) tools to detect objects using high-dimensional sensors such as camera images [1] or point clouds measured by LiDAR [2] have been extensively applied to autonomous vehicles [3], [4]. As ML continues to advance in the area of vision-based autonomous vehicles and more these vehicles are being integrated into society, it is important to ensure the robustness of these systems that rely on various sensor signals in uncertain environments. Analyzing the worst cases within uncertainties has been a useful approach to robustify control systems [5] and reinforcement learning policies [6]. To follow the worst cases approach for robust systems, researchers have revealed the vulnerability of the machine learning methods, especially deep learning tools developed for computer vision tasks (classification and object detection), to data perturbed by adversaries. For example, it was demonstrated that one can add small perturbations to images unnoticeable to human eyes but strong enough to result in incorrect image classifications [7], [8], [9]. Furthermore,

adversarial image perturbations against autonomous vehicles were demonstrated in relatively recent works: (1) Modifying physical objects, such as putting stickers on a road [10] or a road sign [11] to fool an ML image classifier or end-to-end vision-based autonomous car; (2) Fooling object tracking algorithm in autonomous driving systems [12].

Although the aforementioned adversarial image perturbations against autonomous cars [10], [11], [12] successfully revealed weaknesses of the vision-guided navigation in autonomous vehicles, the perturbed images are generated offline in these approaches. The offline methods [11], [12] do not consider the effect of the real-time attack on dynamically changing environments during the driving or flight of the vehicles. To prevent accidents [13] of vision-guided autonomous vehicles or adversarial exploitation that can be attributed to defective perception systems and their vulnerabilities, we need to study attack and defense techniques that go beyond the offline methods for DNNs.

There are two approaches to generating adversarial image perturbations depending on access to the victim perception model. The *white-box* attack approaches generate adversarial image perturbations through iterative optimization given full access to the victim ML classifier (or object detector) [8], [12]. In the *white-box* method, images are the decision variables of optimization, and the training loss function is re-used with incorrect labels set by the adversary. This optimization takes iterative gradient steps with respect to the image variables that are calculated using back-propagation through the known victim ML classifier [8] (or object detector [12]). The *black-box* approaches [14], [15] assume querying input and output pairs of the victim model and estimate gradient, e.g., *Kiefer–Wolfowitz* algorithm [16]. However, estimating the gradients in the *black-box* approaches requires a sufficient number of samples that would not be available from autonomous systems operating in dynamic environments.

In this paper, we adopt the approach in [17] for using generative-neural-network (GNN) that skips the iterative steps in the *white-box* approaches after the network is trained under the generative adversarial network framework [18]. In our proposed framework, the GNN is integrated within the multi-level framework that has several components. First, the GNN acts as an online image generator. Second, a reinforcement learning agent learns to misguide the vehicle according to the adversary’s objective. Lastly, a binary decision-maker chooses when to use image attacks depending on the proficiency of the image attack generator given the current state estimate.

*Research supported by NSF CPS #1932529, NSF CMMI #1663460, and UNR internal funding.

¹Hyung-Jin Yoon and Petros Voulgaris are with the Department of Mechanical Engineering, University of Nevada, Reno, NV 89557, USA {hyungjiny, pvoulgaris}@unr.edu

²Hamidreza Jafarnejadsani is with the Department of Mechanical Engineering, Stevens Institute of Technology, NJ 07030, USA hjafarne@stevens.edu

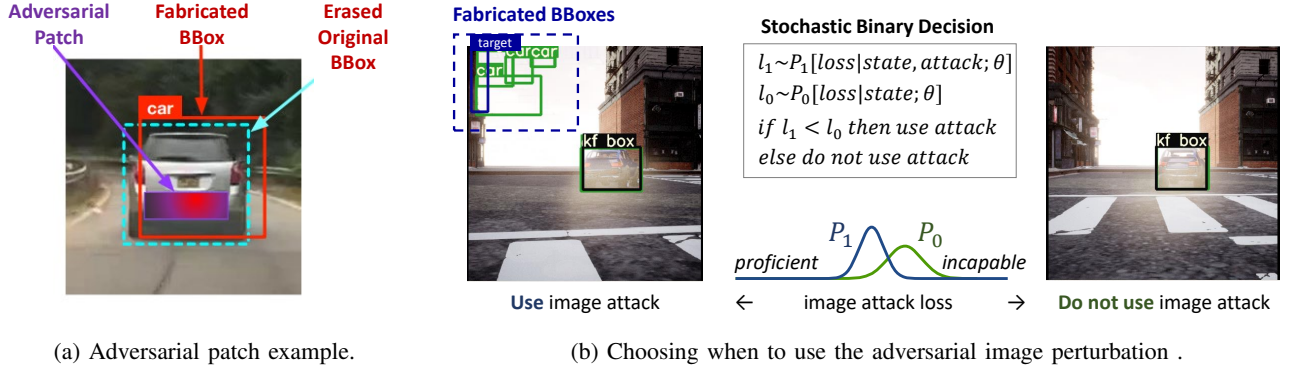


Fig. 1: Image attacks: (a) Adversarial patch in [12], (b) Adversarial perturbation with binary decision in this paper. *kf box* denotes Kalman filtered bounding box (BBox).

II. RELATED WORKS

Adversarial image perturbations to attack autonomous vehicles that use camera images for navigation have been studied in [19], [12], [20]. For example, in [19], an optimization problem was formulated to place black marks on the roads to steer an end-to-end autonomous driving car off the road in a virtual reality environment for testing, following the demonstration of attacking Tesla’s autonomous driving systems with three small stickers [10]. In [12], the authors demonstrated to use a *white-box* adversarial image perturbation method toward an object tracking of an autonomous system that uses *Kalman filter* (KF) in order to disrupt the object tracking. Furthermore, the method in [12] was shown to be effective in attacking an industry-level perception module that uses vision-based object detection fused with LIDAR, GPS, and IMU [20].

Full sets of iterative optimization computations are needed for every new image in the aforementioned results [12], [20] based on the *white-box* methods. Hence, these methods are not suitable for dynamic environments with evolving situations and control loops of the autonomous vehicle. In fact, approaches in [12], [20] do not deal with the varying computation time of the iterative optimizations that might have varying termination steps for online applications. Furthermore, the attack methods in [12], [20] need to use additional state information that is sometimes less accessible than the image stream. For example, in order to generate the adversarial patch in Figure 1a, the attacker needs to know the exact anchor index associated with the target bounding box (BBox) and the place to put the bounding box. As the authors in [12] mentioned in *open review* [21], the adversarial patch area was *manually annotated* in each video frame.

In this paper, we present an image attack framework for vision-guided autonomous vehicles that has multiple learning components (as detailed in Figure 3 that follows). First, a low-level adversarial image perturbation is implemented using a generative network [17]. A binary decision-maker chooses when to attack according to the estimated attack proficiency, as illustrated in Figure 1b. Finally, a state estimation-based reinforcement learning that uses a dynamic auto encoder decides actions that are the coordinates of the fabricated object detection bounding box as shown in Figure 1b.

Compared to the previous works [12], [20] on attacking autonomous vehicles using adversarial image perturbations, our proposed multi-level framework features the following advantages:

- A generative network for adversarial image attack is trained for online image attack that enables the real-time implementation on real-world robots as shown in our experiment, in contrast to the offline implementation in [12].
- In our approach, the state estimation-based reinforcement learning agent chooses the image frame area to fabricate the bounding boxes to achieve adversarial goals in terms of rewards. As a result, this framework does not need manual effort to annotate the patch area as in [12].
- Compared to the noticeable (colorful) adversarial patch in Figure 1a, our image perturbation is less noticeable because the attack signals are saturated within a bound using a scale factor α , and the binary decision-maker would wait until the low-level image attacker is sufficiently trained, as shown in Figure 1b.

III. REAL-TIME ADVERSARIAL IMAGE ATTACK

We aim to develop a solution that can learn to generate adversarial image perturbations in real-time and wait to use the adversarial image attack until the attack generator becomes more proficient in the form of binary decision-making as shown in Figure 1b. The adversarial image perturbations affect the perception of the autonomous vehicles to misguide the vehicles according to the adversary’s objectives. For example, the adversary aims to cause collisions and deviate the vehicle to the left or right. We formulate the problem with the following assumptions and settings.

A. Problem description and proposed framework

We consider autonomous vehicles that follow the target object detected by an object detection model given camera images, as shown in Figure 2. For the object detection model, we used a recent version of *YOLO* [1] downloaded from [22]. The object detector network denoted as **YOLO**(\cdot) maps a camera image into a multi-dimensional tensor output. The output is post-processed into the list of bounding box coordinates using non-max suppression [1]. From the detected

bounding box list, the box of the target class with the greatest confidence is used to generate tracking control commands. The autonomous guidance system uses the vehicle's actuators (acceleration pedal, brake, and steering wheel) to keep the bounding box of the target at the center of the camera view and the size of the bounding box within a range. As a result, the vehicle moves toward and tracks the target.

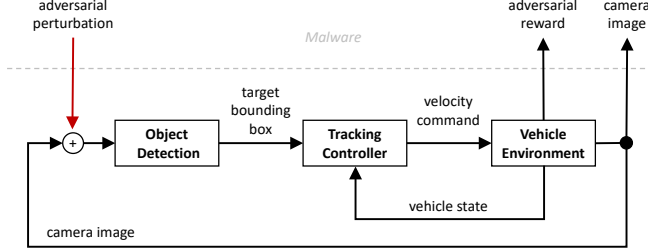


Fig. 2: Attacker (malware) and victim system (guidance)

We assume that the goal of the adversary is to hinder the target tracking control in Figure 2. As shown in Figure 2, It is assumed that the attacker will be embedded as *Malware* that has access to the image stream and perturbs the image stream input to the object detection module of the victim system. Given the image streams denoted as $\{\mathbf{x}_0, \mathbf{x}_1, \dots, \mathbf{x}_t\}$, the goal of the attacker is to generate adversarial image perturbations $\{\mathbf{w}_0, \mathbf{w}_1, \dots, \mathbf{w}_t\}$ that misguides the victim vehicle according to adversarial objectives expressed in terms of adversarial rewards $\{r_1, r_2, \dots, r_t\}$. The reward is a function of the state of the vehicle, such as position, velocity, or collision states and actions that are the coordinates to fabricate the bounding boxes using the image attack generator as shown in Figure 3. The rewards are necessary to apply *reinforcement learning* (RL) that learns the correlation between actions and rewards for different states of the system. In this framework, a binary decision-maker takes the role of choosing when to attack given attack proficiency (represented as loss denoted in Figure 3). The problem considered in this framework is summarized as follows:

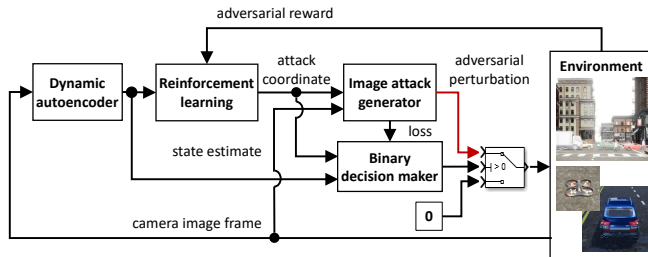


Fig. 3: Image attack framework with binary decision maker.

Problem: Develop machine learning methods that learn to increase the sum of rewards $\{r_t\}$ for the adversary by generating adversarial perturbation $\{\mathbf{w}_t\}$ while selecting when to use the attack as shown in Figure 3. The ML method assumes to use only the image stream $\{\mathbf{x}_t\}$ from the autonomous vehicle that has a guidance system and malware shown in Figure 2.

B. Online image attack with binary decision making

In our framework, the decision whether to use or not to use the adversarial image perturbation depends on the proficiency of the image attack generator. Such binary decision-making belongs to the multi-armed bandit class of problems [23]. In a multi-armed bandit problem, the decision-maker selects the most profitable decision. However, in contrast to the classical multi-armed bandit, where the profits (or rewards) are generated from independent-stationary distributions, the decision-maker in our framework needs to consider the states of the system that are not stationary. To be specific, given the attack coordinate chosen by RL and the state estimate from the dynamic autoencoder, the decision-maker needs to know whether it is profitable to use the attack or not. In [24], deep neural network (DNN) was used to learn the correlation between the state, decision, and profit. In [24], random drop-out [25] with the DNN was used to estimate the distributions of the profits given each decision. The authors in [24] coined the term *Neural Thompson Sampling* (NTS) for the multi-armed bandit algorithm that uses DNN with random dropout.

We attempted to apply the NTS for binary decision-making that considers the proficiency of the image attack generator as the profits of the multiarmed bandit. Although the direct application of NTS to our framework is intuitively appealing, there is an issue of causality. Note that the loss value is independent of binary decision-making. The loss value depends on attack coordinates and the image frame. In the experiment section of this paper, we tested the NTS, and the NTS did not show the desired behavior of choosing to attack when the expected loss value is small.

Therefore, we devised a different method from NTS. The devised method compares two conditional expectations

$$E[l_t | \mathbf{h}_t, \mathbf{a}_t] \quad \text{and} \quad E[l_t | \mathbf{h}_t]. \quad (1)$$

The rationale behind this device is to compare the expected loss given a_t and the expected loss averaged over all the other possible a . If a_t suggested by RL has a lower expected loss than the loss averaged over a_t then the current a_t could be a useful suggestion. We coin this decision-making method as *Conditional Sampling* (CS). The loss estimation and the decision making procedure of CS are described as follows: **Estimation:** The estimation for CS is formulated as the following optimization.

$$\begin{aligned} \arg \min_{\theta^{\text{dec}}} \|l_t - \hat{l}_0(\mathbf{h}_t; \theta^{\text{dec}})\|^2, \\ \arg \min_{\theta^{\text{dec}}} \|l_t - \hat{l}_1(\mathbf{h}_t, \mathbf{a}_t; \theta^{\text{dec}})\|^2, \end{aligned} \quad (2)$$

where l_t denotes the image attack loss value and \mathbf{h}_t denotes state estimate and \mathbf{a}_t denotes the attack coordinates and \hat{l} are DNN trained with dropout sampling. The DNN has the parameter θ^{dec} to be optimized.

Decision making: Given current \mathbf{h}_t and \mathbf{a}_t , sample l_0 and l_1 using the same procedure of NTS that uses Gaussian distribution fit with the output sample perturbed by dropout in DNN, i.e.,

$$l_0 \sim \hat{l}_0(\mathbf{h}_t; \theta^{\text{dec}}) \quad \text{and} \quad l_1 \sim \hat{l}_1(\mathbf{h}_t, \mathbf{a}_t; \theta^{\text{dec}}), \quad (3)$$

where the sampling first fits the output samples of \hat{l} perturbed by the random dropout into a normal distribution and then take as a sample from the random distribution. See [24] for further details of the sampling. Finally, as in NTS, we choose the decision with lower loss value sample, i.e., if $l_0 < l_1$ then $z_t = 0$, otherwise $z_t = 1$. We denote the conditional probability distributions corresponding to the samplings as $P_0[l_t|\mathbf{h}_t]$ and $P_1[l_t|\mathbf{h}_t, \mathbf{a}_t]$ as shown in Figure 1b.

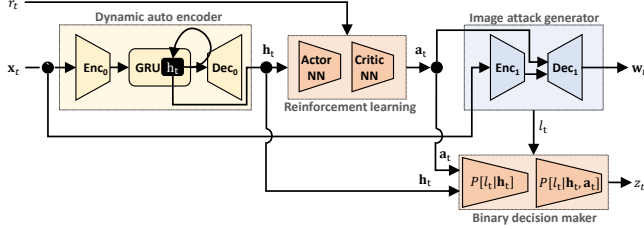


Fig. 4: Multi-level image attack computation network.

Algorithm 1 Recursive Image Attack

Initialize: $t \leftarrow 0$; load the pre-trained parameters of the recursive attack networks.

repeat

Generate attack command using RL policy (Actor)

$\mathbf{a}_t \leftarrow \mathbf{Actor}(\mathbf{h}_t)$

Encode the observed image \mathbf{x}_t from the environment

$\zeta_t \leftarrow \mathbf{Enc}_1(\mathbf{x}_t)$

Generate adversarial image perturbation

$\mathbf{w}_t \leftarrow \mathbf{Dec}_1(\zeta_t, \mathbf{a}_t)$

Feed \mathbf{w}_t to the environment and get new image \mathbf{x}_{t+1}

$\mathbf{x}_{t+1}, \mathbf{s}_{t+1}, r_t, \text{done} \leftarrow \mathbf{Environment}(\mathbf{s}_t, \mathbf{w}_t)$

Recursively update the state predictor \mathbf{h}_{t+1} with \mathbf{x}_{t+1}

$\mathbf{h}_{t+1} \leftarrow \mathbf{GRU}(\mathbf{h}_t, \mathbf{Enc}_0(\mathbf{x}_{t+1}), \mathbf{a}_t)$

Sample from the conditional distribution as in (3), i.e.,

$l_0 \sim P_0[l_t|\mathbf{h}_t]$ and $l_1 \sim P_1[l_t|\mathbf{h}_t, \mathbf{a}_t]$.

Use \mathbf{w}_t if $l_0 < l_1$. Otherwise do not use it.

until done is True, i.e., the episode terminates with a terminal condition.

The estimation models of binary decision making are integrated within the computation networks that consist of DNNs in Figure 4. An advantage of the proposed framework is real-time generation of the adversarial image perturbations due to recursive computations. As shown in Figure 4, image \mathbf{x}_t at time t is fed into encoder networks (\mathbf{Enc}_0 and \mathbf{Enc}_1) for dimension reduction: \mathbf{Enc}_0 for state estimation and \mathbf{Enc}_1 for generating perturbed image \mathbf{w}_t . The dynamic autoencoder consists of \mathbf{Enc}_0 , GRU (that denotes the gated recurrent unit [26]), and \mathbf{Dec}_0 (that denotes a decoder). The GRU uses encoded image $\mathbf{Enc}_0(\mathbf{x}_t)$ and the high-level attack action \mathbf{a}_t to recursively update the hidden state of GRU, \mathbf{h}_t , i.e., $\mathbf{h}_{t+1} = \mathbf{GRU}(\mathbf{h}_t, \mathbf{Enc}_0(\mathbf{x}_t), \mathbf{a}_t)$. The initial value of \mathbf{h}_0 is randomly generated using Normal distribution. The estimated state information in \mathbf{h}_t is used to generate the high level action by the actor (policy), i.e., $\mathbf{a}_t = \mathbf{Actor}(\mathbf{h}_t)$. Then, the adversarial image perturbation is generated by \mathbf{Dec}_1 given \mathbf{a}_t and another encoded image by \mathbf{Enc}_1 , i.e., $\mathbf{w}_t = \mathbf{Dec}_1(\mathbf{Enc}_1(\mathbf{x}_t), \mathbf{a}_t)$. The

perturbed image frame receives the perturbation with a scale factor α , i.e., $\tilde{\mathbf{x}}_t = \max(\min(\mathbf{x}_t + \alpha \mathbf{w}_t, 1), 0)$. Then the decision to use ($z_t = 1$) or not ($z_t = 0$) use the adversarial perturbation \mathbf{w}_t is determined by the conditional sampling (CS) described in (3). The recursive process of generating adversarial image perturbation using only camera image is summarized as Algorithm 1 below. As shown in Algorithm 1, at each time of generating the adversarial perturbation \mathbf{w}_t , the entire computation only uses the current observation or the state values in the previous time-step without iterative optimization. Hence, the algorithm can generate the image attack in real-time. The recursive process of generating adversarial image perturbation using only camera image is summarized in Algorithm 1.

C. Multi-time scale optimization to train the attacker

We use multi-level stochastic optimization that separates the time scales of the updates of the multiple components in Figure 3. The stochastic optimization trains the multi-level image attack computational networks in Figure 4. The learning components and the environment are coupled to each other while simultaneously updating the components' parameters. Different choices of the time scales of the update will result in various behaviors in multi-time scale optimization. For example, actor-critic [27] sets a faster update rate for the critic than the actor. And the generative adversarial network in [28] sets a faster update for the discriminator than the generator. Following the heuristics and theories in [27], [28], we set the slower parameter update rates in lower-level components.

Denote the parameters of the multiple components as follows: θ_n^{img} is the parameter of $\mathbf{Enc}_1(\cdot)$, $\mathbf{Dec}_1(\cdot)$; θ_n^{sys} is the parameter of the dynamic autoencoder consist of $\mathbf{Enc}_0(\cdot)$, $\mathbf{GRU}(\cdot)$, and $\mathbf{Dec}_0(\cdot)$; θ_n^{actor} is the parameter of the actor denoted as $\mathbf{Actor}(\cdot)$; θ_n^{critic} is the parameter of the critic denoted as $Q(\cdot, \cdot)$ that is action-value function for policy evaluation. The parameters are updated with different step sizes according to the pace of the update rates as follows:

$$\begin{aligned} \theta_{n+1}^{\text{img}} &= \theta_n^{\text{img}} + \epsilon_n^{\text{img}} S_n^{\text{img}}(\mathcal{M}_{\text{trajectory}}) \\ \theta_{n+1}^{\text{dec}} &= \theta_n^{\text{dec}} + \epsilon_n^{\text{dec}} S_n^{\text{dec}}(\mathcal{M}_{\text{decision}}) \\ \theta_{n+1}^{\text{actor}} &= \theta_n^{\text{actor}} + \epsilon_n^{\text{actor}} S_n^{\text{actor}}(\mathcal{M}_{\text{transition}}) \\ \theta_{n+1}^{\text{critic}} &= \theta_n^{\text{critic}} + \epsilon_n^{\text{critic}} S_n^{\text{critic}}(\mathcal{M}_{\text{transition}}) \\ \theta_{n+1}^{\text{sys}} &= \theta_n^{\text{sys}} + \epsilon_n^{\text{sys}} S_n^{\text{sys}}(\mathcal{M}_{\text{trajectory}}) \end{aligned} \quad (4)$$

where the update functions S_n^{img} , S_n^{dec} , S_n^{actor} , S_n^{critic} and S_n^{sys} are stochastic gradients with loss functions (to be described in following sections) calculated with data samples from the replay buffers, i.e., $\mathcal{M}_{\text{trajectory}}$, $\mathcal{M}_{\text{transition}}$, and $\mathcal{M}_{\text{decision}}$. The replay buffers store finite numbers of recently observed tuples of $(\mathbf{x}_t, \mathbf{a}_t)$, $(\mathbf{h}_{t-1}, \mathbf{a}_t, r_t, \mathbf{h}_t)$, and $(\mathbf{h}_t, \mathbf{a}_t, l_t)$ into $\mathcal{M}_{\text{trajectory}}$, $\mathcal{M}_{\text{transition}}$, and $\mathcal{M}_{\text{decision}}$ respectively.

The step-sizes: ϵ_n^{img} , ϵ_n^{dec} , $\epsilon_n^{\text{actor}}$, $\epsilon_n^{\text{critic}}$, and ϵ_n^{sys} within our multi-time scale optimization are set as follows. The generation of adversarial image perturbation depends on the generator with parameter θ_n^{img} , the actor that determines the attack coordinates with parameter θ_n^{actor} , and the binary decision maker that choose to use the adversarial perturbation or not with parameter θ_n^{dec} . Seeing that the generation of

the adversarial image perturbation and its use are governed by a policy with parameters θ_n^{img} , θ_n^{actor} , and θ_n^{dec} , we set faster update rates for the parameters relevant to policy evaluation, i.e., θ_n^{critic} , and θ_n^{sys} . Hence, the step size follows the diminishing rules as $n \rightarrow \infty$

$$\frac{\epsilon_n^{\text{img}}}{\epsilon_n^{\text{dec}}} \rightarrow 0 \quad \frac{\epsilon_n^{\text{dec}}}{\epsilon_n^{\text{actor}}} \rightarrow 0 \quad \frac{\epsilon_n^{\text{actor}}}{\epsilon_n^{\text{critic}}} \rightarrow 0 \quad \frac{\epsilon_n^{\text{critic}}}{\epsilon_n^{\text{sys}}} \rightarrow 0, \quad (5)$$

according to our intention to set slower update rates for lower-level components (of the policy) that generate data for upper-level components (of the policy evaluation). In [28], it was shown that the ADAM [29] step size rule can be set to implement the multi-time scale step size rule in (5).

The multi-time scale stochastic optimization is summarized in Algorithm 2 in Appendix. We describe the loss functions of the stochastic gradients for the multi-level stochastic optimization in the following sections.

1) *Image attack generator*: We use a proxy object detector (white box model) to train the attack generator. The proxy object detector YOLOv5 is the recent version of YOLO [1] downloaded from [22]. Let us briefly describe the interface of YOLOv5. Given an image frame \mathbf{x}_t that has the image size 448×448 with RGB channels, The detector network denoted as $\text{YOLO}(\cdot)$ maps an image \mathbf{x}_t into features on grid maps that as anchor points. The features include the coordinate of the bounding box and object classification probabilities [30]. The high dimensional output enables $\text{YOLO}(\cdot)$ to consider many possible classes of objects, shape of bounding box, and coordinates.

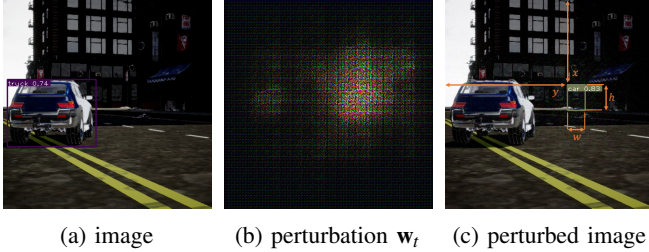


Fig. 5: Fabrication of the bounding box at (x, y, w, h) with \mathbf{w}_t

Our image attack generator injects adversarial perturbation to fabricate bounding boxes at the target coordinate as shown in Figure 1b. Using reinforcement learning, the high-level attacker (reinforcement learning agent) arbitrarily chooses the target coordinates to place the fabricated bounding boxes accordingly. Given the high-level attack $\mathbf{a}_t \in [0, 1] \times [0, 1] \times [0, 1] \times [0, 1]$ representing coordinates x and y of a bounding box, i.e., width and height, the image attack network aims to delete all the other bounding boxes but to keep the one corresponding to the high level attack as illustrated in Figure 5. We could delete the existing bounding box and place a bounding box according to the target coordinates when given enough optimization iterations (500 iterations in Figure 5).

For online image attack, the iterative optimization that fabricated the bounding box as in Figure 5 is not suitable because the optimization needs to perform within a fixed time step of the control loop in the autonomous system. In

our framework, we train the attack generator that minimizes the loss function through the generator, i.e.,

$$\arg \min_{\theta^{\text{img}}} l^{\text{img}}(\mathbf{w}(\mathbf{x}; \theta^{\text{img}}), \mathbf{x}, \mathbf{a}), \quad (6)$$

where $\mathbf{w}(\mathbf{x}; \theta^{\text{img}}) := \text{Dec}_1(\text{Enc}_1(\mathbf{x}; \theta^{\text{img}}), \mathbf{a}; \theta^{\text{img}})$ and \mathbf{x}, \mathbf{a} are sampled from $\mathcal{M}_{\text{trajectory}}$. instead of the optimization over image space that is for one time use, i.e., $\arg \min_{\mathbf{w}} l^{\text{img}}(\mathbf{w}, \mathbf{x}_t, \mathbf{a}_t)$. The stochastic gradient $S_n^{\text{img}}(\mathcal{M}_{\text{trajectory}})$ in (4) is associated with the loss function in (6).

For the loss function in (6), we use the same loss function from [1] to invert the victim object detection network. The loss function of the adversarial perturbation \mathbf{w} given an image \mathbf{x} and an action \mathbf{a} that describe the target bounding box coordinates (x, y, w, h) is as follows:

$$\begin{aligned} l^{\text{adv}}(\mathbf{w}; \mathbf{x}, \mathbf{a}) &= \lambda_{\text{coord}} \sum_{i=1}^3 \sum_{j=1}^{S_i^2} \sum_{k=1}^B \mathbf{1}_{i,j,k}^{\text{obj}} \left[(x - \hat{x}_{i,j,k})^2 + (y - \hat{y}_{i,j,k})^2 \right] \\ &+ \lambda_{\text{coord}} \sum_{i=1}^3 \sum_{j=1}^{S_i^2} \sum_{k=1}^B \mathbf{1}_{i,j,k}^{\text{obj}} \left[(\sqrt{w} - \sqrt{\hat{w}_{i,j,k}})^2 + (\sqrt{h} - \sqrt{\hat{h}_{i,j,k}})^2 \right] \\ &+ \sum_{i=1}^3 \sum_{j=1}^{S_i^2} \sum_{k=1}^B \mathbf{1}_{i,j,k}^{\text{obj}} (1 - \hat{c}_{i,j,k})^2 \\ &+ \lambda_{\text{no obj}} \sum_{i=1}^3 \sum_{j=1}^{S_i^2} \sum_{k=1}^B \mathbf{1}_{i,j,k}^{\text{no obj}} (0 - \hat{c}_{i,j,k})^2 \\ &+ \sum_{i=1}^3 \sum_{j=1}^{S_i^2} \sum_{k=1}^B \mathbf{1}_{i,j}^{\text{no obj}} \sum_{c \in \text{classes}} (p_{i,j,k}(c) - \hat{p}_{i,j,k}(c))^2 \end{aligned} \quad (7)$$

where $\mathbf{1}_{i,j,k}^{\text{obj}} = 1$ if the target object is associated with the grid of the index i, j, k , and otherwise, it is zero. Also, $\mathbf{1}_{i,j,k}^{\text{no obj}} = 1$ if $\mathbf{1}_{i,j,k}^{\text{obj}} = 0$, and otherwise it is zero. In (7), the first two terms are to minimize the error between inferred coordinates of the bounding box and the target coordinates x, y, w, h that are mapped from \mathbf{a}_t through linear equations. The first two terms are added into the loss function with the weight λ_{coord} .

In (7), the third and the fourth term count the error in having a target object associated with each anchor box with index i, j, k . The fourth term is added to the loss function with the weight $\lambda_{\text{no obj}}$. The values of the indicator $\mathbf{1}_{i,j,k}^{\text{obj}}$ given the target coordinate (x, y, w, h) is determined using the following procedure.

First, we select (i', k') through the minimization below

$$i', k' = \arg \min_{i,k} \left(\sqrt{w_{i,k}^{\text{template}}} - \sqrt{w} \right)^2 + \left(\sqrt{h_{i,k}^{\text{template}}} - \sqrt{h} \right)^2$$

Then, the nearest anchor index j' can be found easily from the $S_i \times S_i$ anchor grid using simple discretization, i.e., dividing the coordinates by the strides of the anchor grids. The specific loss function in (6) is described in Appendix.

2) *System identification for state estimation*: The system identification aims to determine the parameter that maximizes the state estimate's likelihood. We maximize the likelihood of state predictor by minimizing the cross-entropy error between

true image streams and the predicted image streams by a stochastic optimization which samples trajectories saved in the memory buffer denoted by $\mathcal{M}_{\text{trajectory}}$ with a loss function to minimize.

The loss function $l^{\text{sys}}(\cdot)$ is calculated using the sampled trajectories from $\mathcal{M}_{\text{trajectory}}$. We calculate the loss function as

$$l^{\text{sys}}(\mathcal{M}_{\text{trajectory}}; \theta_{\text{sys}}) = \frac{1}{M} \sum_{m=1}^M H(\mathbf{X}_m, \hat{\mathbf{X}}_m) \quad (8)$$

where $\mathbf{X}_m = (\mathbf{x}_0, \dots, \mathbf{x}_T)_m$ is the m^{th} sample image stream with time length T . Here, $H(\cdot, \cdot)$ is average of the binary cross-entropy $h(\cdot, \cdot)$ between the original image stream \mathbf{X}_m and the predicted image stream $\hat{\mathbf{X}}_m$ as

$$H(\mathbf{X}_m, \hat{\mathbf{X}}_m) = \frac{1}{TWHC} \sum_{t=1}^T \sum_{i=1}^W \sum_{j=1}^H \sum_{k=1}^C h([\mathbf{X}_m]_{t,i,j,k}, [\hat{\mathbf{X}}_m]_{t,i,j,k})$$

where i, j, k denotes width, height, color index for the image with width W , height H , color channel $C = 3$ and the binary cross entropy $h(\cdot, \cdot)$ calculate the difference between the pixel intensities of $[\mathbf{X}_m]_{t,i,j,k} \in [0, 1]$ and $[\hat{\mathbf{X}}_m]_{t,i,j,k} \in [0, 1]$.¹

We generate the predicted trajectory given the original trajectory with image stream $\mathbf{X}_m = (\mathbf{x}_0, \dots, \mathbf{x}_T)_m$ and action stream $(\mathbf{a}_0, \dots, \mathbf{a}_T)_m$ by processing them through the encoder, GRU, and the decoder as

$$\mathbf{h}_{t+1} = \text{GRU}(\mathbf{h}_t, \text{Encoder}_1(\mathbf{x}_t), \mathbf{a}_t), \quad \mathbf{h}_0 \sim \mathcal{N}(0, \mathbf{I})$$

$$\hat{\mathbf{x}}_{t+1} = \text{Decoder}_1(\mathbf{h}_{t+1})$$

and collect them into $\hat{\mathbf{X}}_m = \{\hat{\mathbf{x}}_1, \dots, \hat{\mathbf{x}}_T\}$. With the loss function in (8), the stochastic gradient for the optimization is defined as

$$S_n^{\text{sys}} = -\nabla_{\theta_{\text{sys}}} l^{\text{sys}}(\mathcal{M}_{\text{trajectory}}; \theta_{\text{sys}}). \quad (9)$$

3) *Actor-Critic policy improvement*: The critic evaluates the policy relying on the principle of optimality [31]. We employed an actor-critic method [32] for the reinforcement learning component in the proposed framework. The critic network is updated using the state estimate \mathbf{h}_t to apply the optimality principle with the following stochastic gradient as

$$S_n^{\text{critic}} = -\nabla_{\theta_{\text{critic}}} l^{\text{critic}}(\mathcal{M}_{\text{transition}}; \theta_{\text{critic}}) \quad (10)$$

with the following loss function²

$$l^{\text{critic}}(\mathcal{M}_{\text{transition}}; \theta^{\text{critic}}) = \frac{1}{M} \sum_{m=1}^M (Q(\mathbf{h}_m, \mathbf{a}_m; \theta^{\text{critic}}) - Q_m^{\text{target}})^2, \quad (11)$$

where $Q_m^{\text{target}} = r_m + \gamma Q(\mathbf{h}'_m, \mu_{\theta}(\mathbf{h}'_m); \theta^{\text{critic}})$ and the state transition samples, i.e., $((\mathbf{h}, \mathbf{a}, \mathbf{h}', r))_0, \dots, (\mathbf{h}, \mathbf{a}, \mathbf{h}', r)_M$, are sampled from the replay buffer $\mathcal{M}_{\text{transition}}$. With the same state transition data samples, we calculate the stochastic gradient for the policy using the estimated policy as

$$S_n^{\text{actor}} = \nabla_{\theta_{\text{actor}}} J(\mathcal{M}_{\text{transition}}; \theta_{\text{actor}}),$$

$$J = \frac{1}{M} \sum_{m=1}^M Q(\mathbf{h}_m, \mu(\mathbf{h}_m; \theta_{\text{actor}}); \theta_{\text{critic}}). \quad (12)$$

¹For $x \in [0, 1]$ and $\hat{x} \in (0, 1)$, the binary cross entropy is calculated as $h(x, \hat{x}) = x \log \hat{x} + (1-x) \log(1-\hat{x})$ and we follow the convention $0 = 0 \log 0$.

²We follow the approach of using target networks in [32] to reduce variance during stochastic updates.

4) *Loss estimator training for the binary decision making*: The stochastic gradient S_n^{dec} in (4) is associated with the loss function described in (2). The stochastic optimization with the aforementioned stochastic gradients is summarized as Algorithm 2.

Algorithm 2 Multi-level Stochastic Optimization

Input: recursive attack Networks in Figure 4,

autonomous vehicle environment, proxy object detector **YOLO**,

Replay buffers: $\mathcal{M}_{\text{trajectory}}$ and $\mathcal{M}_{\text{transition}}$.

Output: Fixed parameters.

Initialize: $t \leftarrow 0$; $n \leftarrow 0$; initialize the parameters of the recursive attack networks.

repeat

repeat

Generate and feed the attack into the environment and update state predictor

$\mathbf{a}_t \leftarrow \mu(\mathbf{h}_t)$

$\mathbf{w}_t \leftarrow \text{Decoder}_1(\text{Encoder}_1(\mathbf{x}_t), \mathbf{a}_t)$

$\mathbf{x}_{t+1}, \mathbf{s}_{t+1}, r_t, \text{done} \leftarrow \text{Environment}(\mathbf{s}_t, \mathbf{w}_t)$

$\mathbf{h}_{t+1} \leftarrow \text{GRU}(\mathbf{h}_t, \text{Encoder}_0(\mathbf{x}_{t+1}), \mathbf{a}_t)$

Add data sample to replay buffers

$\mathcal{M}_{\text{transition}} \leftarrow (\mathbf{h}_t, \mathbf{a}_t, r_t, \mathbf{h}_{t+1})$

$\mathcal{M}_{\text{trajectory}} \leftarrow (\mathbf{x}_t, \mathbf{a}_t)$

Update the parameters with samples from $\mathcal{M}_{\text{transition}}$ and $\mathcal{M}_{\text{transition}}$ using the stochastic update in (4).

$t \leftarrow t + 1$; $n \leftarrow n + 1$

until done is True, i.e., the episode terminates.

Start the next row of $\mathcal{M}_{\text{trajectory}}$ for a new trajectory (episode) and pop-out the oldest trajectory row in the replay buffer.

Reset **Environment** and $t \leftarrow 0$

until the performance meets the requirements.

Fix the parameters.

IV. EXPERIMENTS

We compare our proposed framework against baselines. Note that the iterative optimization-based methods in [12], [20] can not be run in real-time (5 - 20Hz). Hence, we modified the baselines to stop the iterative optimization every time steps of the control loop at 5 Hz. Furthermore, the baseline methods need manual annotation of the mask as described in [21]. Hence, we manually place the target area to fabricate the bounding box according to the adversarial objectives, e.g., putting the bounding box at the left when the adversary needs to move the vehicle to the left. All our experiments consider attacking a vision-based guidance system depicted in Figure 2 that uses *YOLOv5* object detector [22]. The vehicle simulation environment is implemented using a game development editor (*Unreal*) [33] that can build *photo-realistic* 3D environments with a plug-in tool (*AirSim*) [34]. For the attack algorithm implementation, we used the robot operating system (*ROS*) [35] to simultaneously implement the learning the attacker and executing the attack using multiple

A. Simulation results and analysis

Fig. 7: Simulation environments.

Methods	Generative network (Y/N)	State estimator (Y/N)	Attack switch (Y/N)
Iterative Optimization	N	N	N
Generative Attack	Y	N	N
Recursive Attack	Y	Y	N
Thompson Sampling	Y	Y	Y
Conditional Sampling	Y	Y	Y

We compare the proposed framework in the first scenario with the adversarial objective, i.e., moving to the right. We report the performance of the trained attackers (listed in Table I) with the last ten episodes of the entire 200 training episodes in Table II. Compared to the iterative optimization method (baseline), the recursive attack methods have greater terminal rewards, collision rate, and terminal distance. Also, the use of the state estimator improves the performance in terms of terminal rewards. On the other hand, the use of the binary decision-makers (Neural Thompson sampling (NTS) or the proposed conditional sampling) decreases the attack

rates. Our proposed conditional sampling reached lower image attack loss and greater terminal reward than NTS.

To validate the efficacy of the proposed framework with real robots, we implemented the algorithm with a miniature drone (*Tello*) [36] as depicted in Figure 6. The miniature drone uses IMU, optical-flow, and barometer to estimate the velocity and follow the velocity commands. We connect the miniature drone to a desktop computer through wifi-networks as shown in Figure 8 (illustrative video is available at the link⁴). The goal of the online image training is to crash the UAV by teaching to fabricate the bounding box. Unlike the simulation environment, we cannot run many training episodes because of the limited battery capacity and hardware damage due to collision. Therefore, we ran a single training episode. In the linked video, the online training took only ten minutes until the UAV crashed.

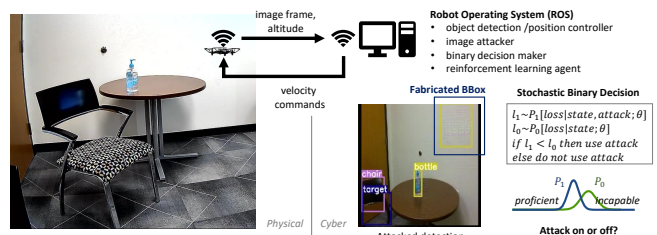


Fig. 8: Attacking UAV’s visual-tracking of a bottle.

V. CONCLUSION

This work showed a new online image attack framework that improves the iterative optimization-based methods that are more suitable for offline attack generation. In our proposed framework, the image attacks can be generated in real-time using only the image stream collected from the autonomous vehicle. Furthermore, the proposed conditional sampling for the binary decision making whether to use the attack (or not) improves the stealthiness by waiting until the proficiency increases. This work will serve as a stepping stone towards strengthening the perception in autonomous vehicles by learning worst-case attack scenarios.

REFERENCES

- [1] J. Redmon, S. Divvala, R. Girshick, and A. Farhadi, “You only look once: Unified, real-time object detection,” in *Proceedings of the IEEE conference on computer vision and pattern recognition*, 2016, pp. 779–788.
- [2] C. R. Qi, H. Su, K. Mo, and L. J. Guibas, “Pointnet: Deep learning on point sets for 3d classification and segmentation,” in *Proceedings of the IEEE conference on computer vision and pattern recognition*, 2017, pp. 652–660.
- [3] (2016) DJI mavic active tracking. Accessed: 2021-12-01. [Online]. Available: <https://youtu.be/s0J0dAI1DM>
- [4] Waymo, “What’s next,” <https://waymo.com/intl/en-us/dataset-whats-next/>, accessed: 2022-02-14.
- [5] T. Başar and P. Bernhard, *H-infinity optimal control and related minimax design problems: a dynamic game approach*. Springer Science & Business Media, 2008.

⁴Crashing indoor UAV at <https://youtu.be/4w0pvQRCVHc>

Environments	Methods	Attack rate (%)	SSIM loss (10^{-2} , avg)	L2 loss (10^{-4} , avg)	Collision rate (%)	Episode length (steps, avg)	Terminal reward (avg \pm stdev)	Time AVG reward (avg \pm stdev)
Drone to a car	Normal	-	-	-	0	90	15.7 \pm 0.0	1.29 \pm 0.07
	Iterative Optimization	100	13.6	12.1	0	91	15.7 \pm 0.1	1.29 \pm 0.07
	Generative attack	\uparrow	8.74	3.94	74	51	30.1 \pm 8.3	2.58 \pm 0.80
	Recursive attack	\uparrow	17.4	7.61	76	60	29.7 \pm 8.1	2.16 \pm 0.45
	Neural Thompson	31.7	6.81	2.58	0	90	21.5 \pm 10.5	1.64 \pm 0.49
	Conditional Sampling	55.3	9.15	4.11	52	77	27.8 \pm 9.2	2.16 \pm 0.57
Cars and trucks	Normal	-	-	-	0	90	1.8 \pm 1.8	0.10 \pm 0.15
	Iterative Optimization	100	16.7	30.3	0	91	-0.4 \pm 2.3	-0.03 \pm 0.13
	Generative attack	\uparrow	7.52	2.68	18	51	5.4 \pm 13.3	0.29 \pm 0.75
	Recursive attack	\uparrow	7.26	2.74	36	60	9.4 \pm 6.3	0.87 \pm 0.43
	Neural Thompson	49.3	4.94	1.77	8	90	6.0 \pm 9.2	0.25 \pm 0.46
	Conditional Sampling	42.7	1.97	0.81	20	77	2.6 \pm 10.6	0.10 \pm 0.53
Following a car	Normal	-	-	-	0	500	0 \pm 0	4.25 \pm 0.04
	Iterative Optimization	100	9.17	7.58	30	293	3.0 \pm 4.6	4.17 \pm 0.23
	Generative attack	\uparrow	5.96	3.16	66	147	7.0 \pm 4.4	2.92 \pm 1.10
	Recursive attack	\uparrow	4.88	2.61	74	49	7.4 \pm 4.4	2.92 \pm 1.33
	Neural Thompson	33.5	1.66	0.96	52	345	5.2 \pm 5.0	4.01 \pm 0.39
	Conditional Sampling	72.8	3.10	2.06	76	214	7.6 \pm 4.3	4.27 \pm 3.54

TABLE II: Ablation study with the last 10 episodes in 5 random training experiments, i.e., $N = 50$.

- [6] L. Pinto, J. Davidson, R. Sukthankar, and A. Gupta, “Robust adversarial reinforcement learning,” in *International Conference on Machine Learning*. PMLR, 2017, pp. 2817–2826.
- [7] A. Kurakin, I. J. Goodfellow, and S. Bengio, “Adversarial machine learning at scale,” in *5th International Conference on Learning Representations, ICLR 2017, Toulon, France, April 24-26, 2017, Conference Track Proceedings*. OpenReview.net, 2017. [Online]. Available: <https://openreview.net/forum?id=BJm4T4Kgx>
- [8] —, “Adversarial examples in the physical world,” in *5th International Conference on Learning Representations, ICLR 2017, Toulon, France, April 24-26, 2017, Workshop Track Proceedings*. OpenReview.net, 2017. [Online]. Available: <https://openreview.net/forum?id=HJGU3Rodl>
- [9] I. J. Goodfellow, J. Shlens, and C. Szegedy, “Explaining and harnessing adversarial examples,” *arXiv preprint arXiv:1412.6572*, 2014.
- [10] E. Ackerman, “Three small stickers in intersection can cause tesla autopilot to swerve into wrong lane,” *IEEE Spectrum*, April, vol. 1, 2019.
- [11] K. Eykholt, I. Evtimov, E. Fernandes, B. Li, A. Rahmati, C. Xiao, A. Prakash, T. Kohno, and D. Song, “Robust physical-world attacks on deep learning visual classification,” in *Proceedings of the IEEE Conference on Computer Vision and Pattern Recognition*, 2018, pp. 1625–1634.
- [12] Y. Jia, Y. Lu, J. Shen, Q. A. Chen, Z. Zhong, and T. Wei, “Fooling detection alone is not enough: First adversarial attack against multiple object tracking,” in *International Conference on Learning Representations (ICLR)*, 2020.
- [13] “Tesla crash driver posted videos of himself riding without hands on wheel,” *The Guardian*, Mar 15, 2021. [Online]. Available: <https://www.theguardian.com/us-news/2021/may/15/tesla-fatal-california-crash-autopilot>
- [14] A. Ilyas, L. Engstrom, A. Athalye, and J. Lin, “Black-box adversarial attacks with limited queries and information,” in *International Conference on Machine Learning*, 2018, pp. 2137–2146.
- [15] Z. Wei, J. Chen, X. Wei, L. Jiang, T.-S. Chua, F. Zhou, and Y.-G. Jiang, “Heuristic black-box adversarial attacks on video recognition models,” in *AAAI*, 2020, pp. 12 338–12 345.
- [16] J. Kiefer, J. Wolfowitz *et al.*, “Stochastic estimation of the maximum of a regression function,” *The Annals of Mathematical Statistics*, vol. 23, no. 3, pp. 462–466, 1952.
- [17] C. Xiao, B. Li, J.-Y. Zhu, W. He, M. Liu, and D. Song, “Generating adversarial examples with adversarial networks,” in *Proceedings of the 27th International Joint Conference on Artificial Intelligence*, 2018, pp. 3905–3911.
- [18] I. Goodfellow, J. Pouget-Abadie, M. Mirza, B. Xu, D. Warde-Farley, S. Ozair, A. Courville, and Y. Bengio, “Generative adversarial nets,” in *Advances in neural information processing systems*, 2014, pp. 2672–2680.
- [19] A. Boloor, K. Garimella, X. He, C. Gill, Y. Vorobeychik, and X. Zhang, “Attacking vision-based perception in end-to-end autonomous driving models,” *Journal of Systems Architecture*, vol. 110, p. 101766, 2020.
- [20] S. Jha, S. Cui, S. Banerjee, J. Cyriac, T. Tsai, Z. Kalbarczyk, and R. K. Iyer, “MI-driven malware that targets av safety,” in *2020 50th Annual IEEE/IFIP International Conference on Dependable Systems and Networks (DSN)*. IEEE, 2020, pp. 113–124.
- [21] (2021) Fooling Detection Alone is Not Enough: Adversarial Attack against Multiple Object Tracking. Accessed: 2021-12-01. [Online]. Available: <https://openreview.net/forum?id=rJl31TNYPr>
- [22] (2021) YOLOv5 — Pytorch. Accessed: 2021-12-01. [Online]. Available: https://pytorch.org/hub/ultralytics_yolov5
- [23] J. Vermorel and M. Mohri, “Multi-armed bandit algorithms and empirical evaluation,” in *European conference on machine learning*. Springer, 2005, pp. 437–448.
- [24] W. Zhang, D. Zhou, L. Li, and Q. Gu, “Neural thompson sampling,” *arXiv preprint arXiv:2010.00827*, 2020.
- [25] Y. Gal and Z. Ghahramani, “Dropout as a bayesian approximation: Representing model uncertainty in deep learning,” in *international conference on machine learning*. PMLR, 2016, pp. 1050–1059.
- [26] K. Cho, B. Van Merriënboer, D. Bahdanau, and Y. Bengio, “On the properties of neural machine translation: Encoder-decoder approaches,” *arXiv preprint arXiv:1409.1259*, 2014.
- [27] V. R. Konda and J. N. Tsitsiklis, “Actor-critic algorithms,” in *Advances in neural information processing systems*, 2000, pp. 1008–1014.
- [28] M. Heusel, H. Ramsauer, T. Unterthiner, B. Nessler, and S. Hochreiter, “Gans trained by a two time-scale update rule converge to a local nash equilibrium,” in *Advances in neural information processing systems*, 2017, pp. 6626–6637.
- [29] D. P. Kingma and J. Ba, “Adam: A method for stochastic optimization,” in *International Conference on Learning Representations (ICLR)*, 2015.
- [30] J. Redmon and A. Farhadi, “Yolo9000: better, faster, stronger,” in *Proceedings of the IEEE conference on computer vision and pattern recognition*, 2017, pp. 7263–7271.
- [31] R. Bellman, “Dynamic programming,” *Science*, vol. 153, no. 3731, pp. 34–37, 1966.
- [32] T. P. Lillicrap, J. J. Hunt, A. Pritzel, N. Heess, T. Erez, Y. Tassa, D. Silver, and D. Wierstra, “Continuous control with deep reinforcement learning,” in *4th International Conference on Learning Representations, ICLR 2016, San Juan, Puerto Rico, May 2-4, 2016, Conference Track Proceedings*, Y. Bengio and Y. LeCun, Eds., 2016. [Online]. Available: <http://arxiv.org/abs/1509.02971>
- [33] (2021) Unreal Engine. Accessed: 2021-12-01. [Online]. Available: <https://www.unrealengine.com/>
- [34] S. Shah, D. Dey, C. Lovett, and A. Kapoor, “Airsim: High-fidelity visual and physical simulation for autonomous vehicles,” in *Field and Service Robotics*, 2017. [Online]. Available: <https://arxiv.org/abs/1705.05065>
- [35] Stanford Artificial Intelligence Laboratory *et al.*, “Robotic operating system,” 2018. [Online]. Available: <https://www.ros.org>
- [36] (2021) DJI Tello. Accessed: 2021-12-01. [Online]. Available: <https://store.dji.com/shop/tello-series>

APPENDIX

A. Simulation environment settings.

1) Environment 1: Moving an UAV away from the scene:

The first scenario of image attack is on a UAV moving towards a car at an intersection, as shown in Figure 10a. In normal operation, the UAV stops at the detected target as shown in Figure 10b. In this scenario, the attacker's goal is to hinder the tracking controller and eventually move the UAV away from the target. Therefore, the reward function is set to promote the desired behavior as

$$r(s_t, \mathbf{a}_t) = \begin{cases} \text{distance from the target} & \text{if done} \\ \text{speed of the UAV} & \text{otherwise.} \end{cases}$$

We use the following termination conditions

$$\text{done}(s_t, \mathbf{a}_t) = \begin{cases} \text{True} & \text{if distance from the target} > 40 \text{ m} \\ \text{True} & \text{if speed of the UAV} < 0.1 \text{ m/s} \\ \text{True} & \text{if the UAV collides} \\ \text{False} & \text{otherwise.} \end{cases}$$

It can be seen from the above reward function that the best possible reward is 40 when the UAV moves away from the target greater than 40 m. And on normal tracking without image attack, the UAV moves to the target and stops at the distance of 15 m from that target. After every termination, the UAV restarts from an initial position with a bounded random position displacement, i.e., uniformly random from $[-2.5, 2.5]$ for the vertical position and from $[-5, 5]$ for the lateral position.

2) Environment 2: Moving an UAV to a lateral direction:

The second scenario of image attack is also on a UAV moving toward a car at an intersection. There are more cars and two people at the intersection compared to the previous scenario as shown in Figure 11a. The UAV moves to a car that has the greatest detection-confidence out of the 5 ground vehicles as shown in Figure 11b. In normal operation, the UAV stops at the target. Similar to the previous scenario, the attacker's goal is to hinder the tracking controller and eventually move the UAV to a designated lateral direction (left or right). Therefore, the reward function is set to promote the desired behavior as

$$r(s_t, \mathbf{a}_t) = \begin{cases} \text{lateral coordinate} & \text{if done} \\ \text{lateral velocity} & \text{otherwise.} \end{cases}$$

It can be seen from the above reward function that the desired behavior attained by maximizing the reward is to move in a direction that maximizes the lateral coordinate, i.e., moving to the left. We used the same termination conditions as Environment 1.

We tested a variation of the scenario to see whether the attacker behaves differently for different setting of reward function. Instead of making the UAV move to the left, we set the reward function to move the UAV to the right. The new reward function is as follows:

$$r(s_t, \mathbf{a}_t) = \begin{cases} -\text{lateral coordinate} & \text{if done} \\ -\text{lateral velocity} & \text{otherwise.} \end{cases}$$

As the learning curves show in Figure 9, the two different reward function results in different terminal positions (left vs. right).

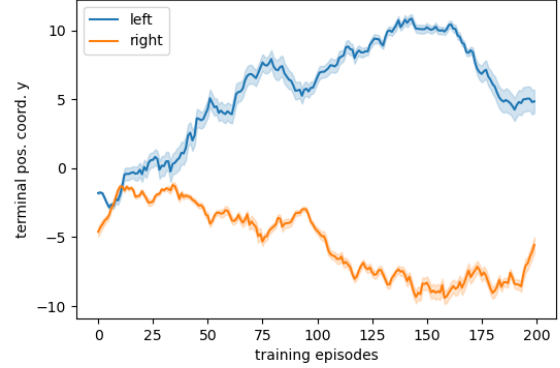


Fig. 9: Effects of the two reward functions: Left vs. Right.

3) Environment 3: Collision of a car follower using Kalman filtered object detections: In this scenario, we tested the attacker's capability with an object detection strengthened using a Kalman filter. As shown in Figure 12a, we simulated a car chasing scenario where the guidance system uses a filtered bounding box in Figure 12b using a Kalman filter (KF), similar to the KF used with an object detector in a previous work [12]. In normal operation, the autonomous car follows the car at the front. In this scenario, the attacker's goal is to cause a collision by fooling the object tracking. For this goal, we used the following reward function as

$$r(s_t, \mathbf{a}_t) = \begin{cases} 10 + \text{speed of the car} & \text{if the car collides} \\ \text{speed of the car} & \text{otherwise.} \end{cases}$$

We also used the following termination conditions

$$\text{done}(s_t, \mathbf{a}_t) = \begin{cases} \text{True} & \text{if the car collides} \\ \text{True} & \text{if speed of the car} < 0.1 \text{ m/s} \\ \text{False} & \text{otherwise.} \end{cases}$$

B. Learning Curves.

We ran five random reinforcement learning experiments and plotted its average and 0.1 standard deviation bounds as shaded areas shown in Figure 13a, b, and c. In the learning curves, we plotted terminal rewards since the attackers in the above scenarios aim to misguide the vehicles into certain terminal states. As we have previously seen in Table II, the image attackers denoted as *Recursive Attack* and *Generative Attack* have greater performance. *Recursive Attack* and *Generative Attack* always use image attacks because they do not have attack switches, as shown in Table I. However, our proposed method that is to decide when to use an attack for stealthy and effective attacks. The learning curves show *Conditional Sampling* has performance comparable to *Recursive Attack* that always uses attacks. Especially, Figure 13b shows *Conditional Sampling* has similar performance to *Recursive Attack*.

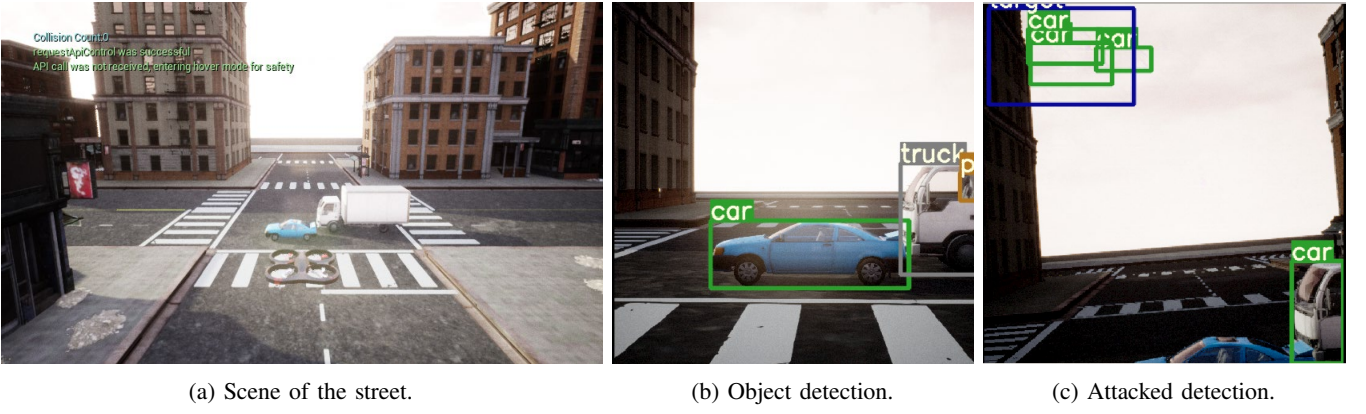


Fig. 10: The UAV moves to the blue car as shown in (a) using the bounding box in (b). The attacker adds image perturbation to place new bounding boxes as shown in (c).

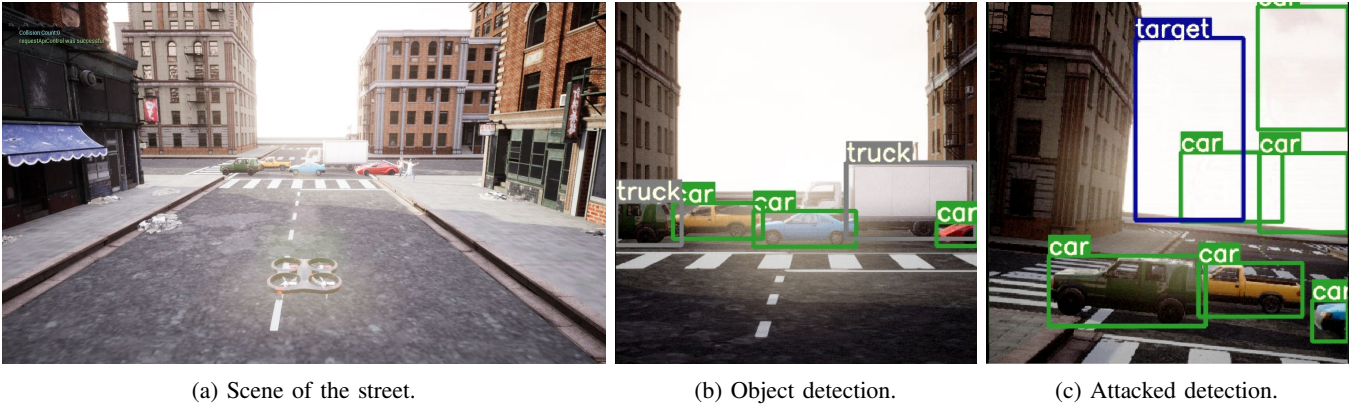


Fig. 11: The UAV moves to a car that has the greatest detection-confidence as shown in (a) using the bounding box in (b). The attacker adds image perturbation to place new bounding boxes as shown in (c).



Fig. 12: The autonomous car follows the front car as shown in (a) using a Kalman filtered bounding box denoted as *kf box* in (b). The attacker adds image perturbations to place new bounding boxes as shown in (c).

C. Attack rates given image attack loss

The proposed methods aim to use the attack when it is good timing. We plot the attack rate vs. image attack loss using the data collected during the training. The proposed method, *Conditional Sampling*, uses the attack when the attack loss is relatively low as shown in Figure 14a, b, and c, compared to *Thompson sampling*. In Figure 14a and b, *Conditional*

Sampling shows negative correlations meaning that it uses more attack when the image attack loss is lower, as intended. However, *Thompson Sampling* in Figure 14a and b shows positive correlations that are to use more attacks when the image attack loss is higher. The correlation coefficients and their p-values are listed in Table III. This unintended behavior of *Thompson Sampling* could be due to the fact that the image

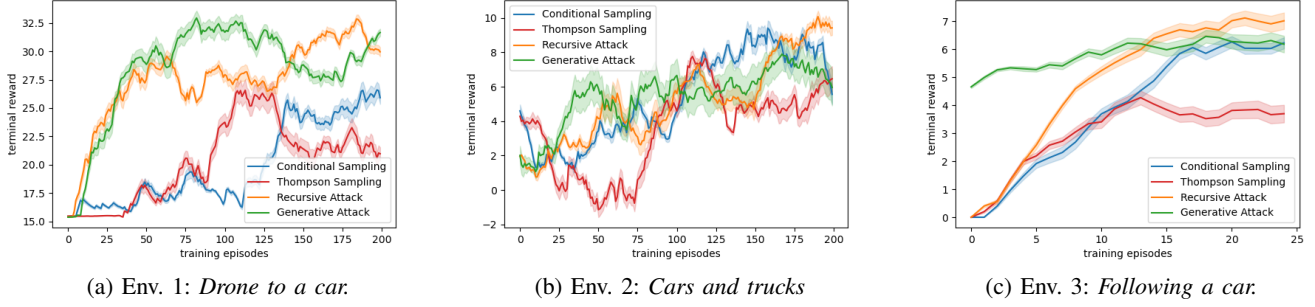


Fig. 13: Reinforcement Learning - Learning curves in terms of terminal rewards.

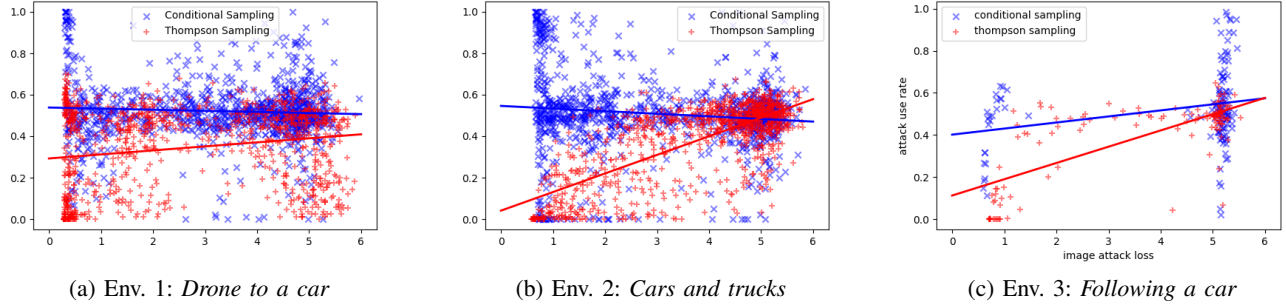


Fig. 14: Attack rate vs. image attack loss

attack loss is independent of the binary decision-making as we described in Section III-B.

	Methods	correlation coefficient	p-value (2-tailed)
Env 1. <i>Drone to a car</i>	Conditional Sampling	-0.06	0.07
	Thompson Sampling	0.19	$p < 0.001$
Env 2. <i>Cars and trucks</i>	Conditional Sampling	-0.11	$p < 0.001$
	Thompson Sampling	0.73	$p < 0.001$
Env 3. <i>Following a car</i>	Conditional Sampling	0.26	0.003
	Thompson Sampling	0.73	$p < 0.001$

TABLE III: Correlation between image attack rate and loss.

D. Parameter selection of the baseline

The baseline method described in Section IV uses iterative optimization having image tensor as a decision variable following the approach in [12], [20]. The performance of the baseline depends on the number of iterations in the optimization. Also, the scale factor α in III-B limits size of the adversarial perturbation $\alpha \mathbf{w}_t$, i.e., $\tilde{\mathbf{x}}_t = \max(\min(\mathbf{x}_t + \alpha \mathbf{w}_t, 1), 0)$. So, we performed parameter sweeping to choose workable parameters of the number of iterations and α as shown in Figure 15. Figure 15 shows the terminal rewards with the baseline methods in Environment 3.

In Figure 15, we see that the baseline method needs to use about 80% of the RGB pixel value, i.e., $\alpha = 0.8$, for effective attacks. Also, it looks that using a large number of iterations is not effective. With a large number of iterations, the resultant adversarial perturbation becomes obsolete because the update of the adversarial patch was generated with the image input taken tens of seconds ago. The final choice of the parameter

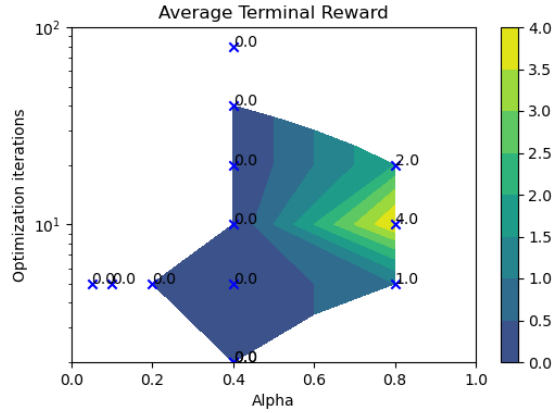


Fig. 15: Parameter sweeping to select α and number of iterations.

for the baseline in Table II is $\alpha = 0.9$ and the number of iterations at 20 steps.